Antiviral Research 97 (2013) 356–368

Contents lists available at SciVerse ScienceDirect

Antiviral Research

journal homepage: www.elsevier.com/locate/antiviral

Resolution of the interaction mechanisms and characteristics of non-nucleoside inhibitors of hepatitis C virus polymerase

Johan Winquist [a], Eldar Abdurakhmanov [a], Vera Baraznenok [b], Ian Henderson [b], Lotta Vrang [b], U. Helena Danielson [a,*]

[a] Department of Chemistry – BMC, Uppsala University, P.O. Box 576, SE-751 23 Uppsala, Sweden
[b] Medivir AB, P.O. Box 1086, SE-141 22 Huddinge, Sweden

ARTICLE INFO

Article history:
Received 10 September 2012
Revised 11 December 2012
Accepted 15 December 2012
Available online 7 January 2013

Keywords:
HCV
NS5B
Inhibitor
Kinetics
Chemodynamics
Thermodynamics

ABSTRACT

Development of allosteric inhibitors into efficient drugs is hampered by their indirect mode-of-action and complex structure–kinetic relationships. To enable the design of efficient allosteric drugs targeting the polymerase of hepatitis C virus (NS5B), the interaction characteristics of three non-nucleoside compounds (filibuvir, VX-222, and tegobuvir) inhibiting HCV replication via NS5B have been analyzed. Since there was no logical correlation between the anti-HCV replicative and enzyme inhibitory effects of the compounds, surface plasmon resonance biosensor technology was used to resolve the mechanistic, kinetic, thermodynamic and chemodynamic features of their interactions with their target and their effect on its interaction with RNA. Tegobuvir could not be seen to interact with NS5B at all while filibuvir interacted in a single reversible step (except at low temperatures) and VX-222 in two serial steps, interpreted as an induced fit mechanism. Both filibuvir and VX-222 interfered with the interaction between NS5B and RNA. They competed for binding to the enzyme, suggesting that they had a common inhibition mechanism and identical or overlapping binding sites. The greater anti-HCV replicative activity of VX-222 over filibuvir is hypothesized to be due to a greater allosteric conformational effect, resulting in the formation of a less catalytically competent complex. In addition, the induced fit mechanism of VX-222 gives it a kinetic advantage over filibuvir, exhibited as a longer residence time. These insights have important consequences for the selection and optimization of new allosteric NS5B inhibitors.

1. Introduction

The WHO estimates that 130–170 million people are currently infected by hepatitis C virus (HCV)[1] worldwide (WHO fact sheet, 2011). The virus was discovered to be the agent responsible for non-A, non-B hepatitis in 1989. It was anticipated that by using a similar strategy as successful for HIV/AIDS, effective drugs would quickly reach the market. However, the discovery process was unexpectedly challenging and specific agents against HCV infection were first approved by the FDA in the spring of 2011 (see Butt and Kanwal, 2012, and references within). Today, two NS3 protease inhibitors (boceprevir and telaprevir) are available for clinical use. They will be used in combination with the former standard of care, the general antiviral ribavirin and pegylated interferon (Butt and Kanwal, 2012).

However, there is a need for additional drugs with alternative modes-of-action due to the high genetic variability of HCV. This does not only affect the pathology of the disease and the susceptibility to therapy (Chayama and Hayes, 2011) but also resistance development (e.g. Imhof and Simmonds, 2011). It is therefore encouraging that additional anti-HCV compounds are currently in clinical trials. Of these, non-nucleotide inhibitors that target allosteric binding sites of the HCV RNA-dependent RNA polymerase (NS5B) are anticipated to be particularly good complements to the protease inhibitors in the clinic, in analogy with the combination treatments used for HIV/AIDS (Granich et al., 2010).

The focus of this study has been to elucidate the characteristics of non-nucleoside inhibitors of HCV NS5B in order to understand the advantages and limitations of these compounds as well as how the next generation of inhibitors should be designed and optimized. We have previously studied the characteristics of early HCV NS5B leads and shown that they bound non-specifically and with

* Corresponding author.
E-mail address: helena.danielson@kemi.uu.se (U.H. Danielson).

[1] *Abbreviations:* AIDS, acquired immunodeficiency virus; CC_{50}, half maximal cytotoxic concentration; DEPC, diethylpyrocarbonate; DMEM, Dulbecco's modified Eagle's medium; DMSO, dimethyl sulfoxide; DSF, differential scanning fluorometry; DTT, 1,4-dithiothreitol (Cleland's reagent); EC_{50}, half maximal effective concentration; EDC, N-ethyl-N'-(3-dimethylaminopropyl)-carbodiimide; FDA, U.S. food and drug administration; HCV, hepatitis C virus; HIV, human immunodeficiency virus; IMAC, immobilized metal affinity chromatography; IPTG, isopropyl β-D-1-thiogalactopyranoside; NHS, N-hydroxysuccinimide; NS5B, non-structural protein 5B; RU, response unit(s); SPR, surface plasmon resonance; TB, terrific broth; T_m, melting temperature.

0166-3542/$ - see front matter © 2013 Elsevier B.V. All rights reserved.
http://dx.doi.org/10.1016/j.antiviral.2012.12.027

low affinity. Here we studied filibuvir (PF-00868554 (Beaulieu, 2010)), VX-222 (VCH222), and tegobuvir (GS 9190 (Vliegen et al., 2009)) – all small non-nucleoside inhibitors that have reached phase II clinical trials (Fig. 1). Although filibuvir and VX-222 are known to convey their inhibitory effect through the allosteric thumb-II site (Li et al., 2009), the mechanism of tegobuvir was uncertain at the start of our studies although resistance mutations had indicated that it acted through the β-hairpin region (amino acids 435–455) in the palm-II site (Shih et al., 2011). However, for all three inhibitors, a deeper understanding of their interaction with their target or inhibition mechanisms was lacking.

A challenge when characterizing allosteric inhibitors is their indirect mode-of-action and the difficulty to establish if compounds are ineffective due to low affinity interactions with the allosteric binding site or if they interact with high affinity but are inefficient in interfering with the catalytic activity of the enzyme. In the case of polymerase inhibitors, an additional complexity is the enzymatic mechanism that involves a template, a primer and four different substrates, and a mechanism that may require a priming step or that is processive. The exact inhibition mechanism of allosteric polymerase inhibitors can therefore be complex and difficult to establish experimentally.

Here we have focused on characterizing the interaction between the inhibitor and the enzyme, whereby any complexities relating to the catalytic cycle can be disregarded. It is therefore possible to establish if the inhibitor is well designed for the purpose of interacting with the target, the feature that can be expected to be amenable to design by medicinal chemists. We have primarily used surface plasmon resonance (SPR) biosensor technology for this purpose (Danielson, 2009). It is a strategy we have previously used for analysis of interactions between HCV NS5B and RNA (Simister et al., 2009), and between HCV and NS3 protease inhibitors (Geitmann et al., 2011). Moreover, in a series of studies, we have demonstrated that it is very useful in the characterization of allosteric inhibitors of HIV reverse transcriptase, another polymerase, for which we have elucidated the relationships between inhibition, interaction mechanism, kinetics, resistance and antiviral effect (Elinder et al., 2010; Geitmann and Danielson, 2007; Geitmann et al., 2006a,b).

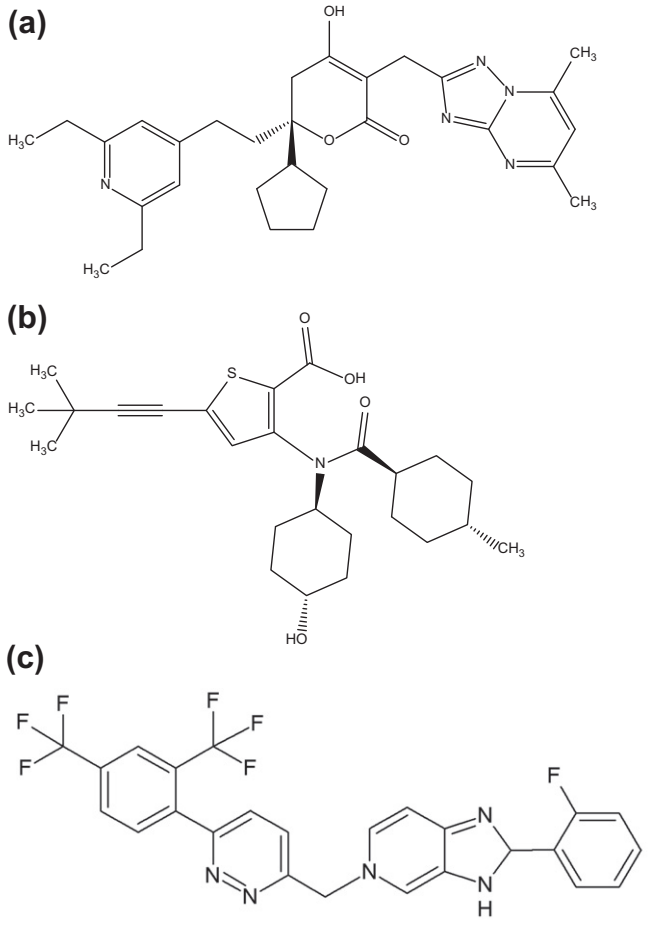

Fig. 1. Structures of (a) filibuvir (PF-00868554), (b) VX-222, and (c) tegobuvir (GS-9190).

The results show that both filibuvir and VX-222 bind directly to NS5B and interfere with the ability of the enzyme to interact with RNA, but that VX-222 has a mechanistic and kinetic advantage over filibuvir, potentially explaining why the compound has a much lower EC_{50} in cell culture (assuming that they have similar uptake). There was no evidence that tegobuvir interacted with NS5B at all.

2. Materials and methods

2.1. Enzyme and inhibitors

The HCV NS5B gene of a Con 1-strain isolate, subtype 1b, was used. Codons corresponding to the C-terminal 21 amino acid transmembrane region were exchanged for a hexa histidine tag coding sequence, and the construct was inserted into a pET21b plasmid between the NheI/XhoI restriction sites. The recombinant enzyme is referred to as NS5Bd21.

The production was based on a protocol of Love et al. (2003). In brief, transformed BL21 Star (DE3) cells were grown in TB media at 37 °C to an OD_{600} value of 1.6 when the cells were shifted to 20 °C. After 45 min, the NS5Bd21 expression was induced by addition of IPTG to a final concentration of 0.4 mM and the cells were let to express overnight. A cell disruptor lysed the cells in 20 mM Tris pH 8.0, 5 mM $MgCl_2$, 300 mM NaCl, 10% glycerol, 10 mM 2-mercaptoethanol, and Complete EDTA free protease inhibitor cocktail tablets (Roche Diagnostics Scandinavia, Stockholm, Sweden). The homogenate was centrifuged at 45000 rcf for 30 min at 4 °C. The cleared lysate was subjected to IMAC (Ni Sepharose 6 Fast Flow, GE Healthcare, Uppsala, Sweden) and elution was performed in one step with 250 mM imidazole. The eluted fractions were pooled and dialysed against 10 mM HEPES–NaOH pH 7.5, 350 mM NaCl, 10% glycerol, 10 mM BME. The sample was applied to a HiTrap SP HP ion-exchange column (GE Healthcare) and NS5Bd21 fractions obtained by gradient elution using 0.35–1.0 M NaCl were collected. Sodium dodecyl sulfate polyacrylamide gel electrophoresis (SDS–PAGE) was used to verify that the obtained protein was of high purity.

Filibuvir (PF-00868554, from Pfizer) was synthesized according to the procedure described by Li et al. (2009), VX-222 (from Vertex) according to the international patent application WO2008/058393, while tegobuvir (aka GS-9190, from Gilead, scaffold presented in (Love et al., 2003)) was synthesized according to the US patent application US2010/0324059. All compounds had >95% purity as assessed by HPLC.

2.2. Cytotoxicity assay

Huh7 hepatocellular carcinoma cells were maintained in DMEM (Invitrogen/Gibco, Stockholm, Sweden) supplemented with 10% heat inactivated fetal calf serum, penicillin (50 U/ml) and streptomycin (50 μg/ml). Briefly, cells were passaged into 96 well microplates (2×10^4 cells/well) and the next day, filibuvir was added in five-fold serial dilutions. After 4 days of incubation at 37 °C, the number of viable cells in each well was assessed by using a soluble XTT formazan assay (Weislow et al., 1989) and the concentration causing 50% decrease in cell viability (CC_{50}) was determined.

2.3. Anti HCV activity assay

Huh-Luc Neo cells (used under license from ReBLikon GmbH, Schriesheim, Germany) were maintained in DMEM (Invitrogen/Gibco, Stockholm, Sweden) supplemented with 10% heat inactivated fetal calf serum, penicillin (50 U/ml), streptomycin (50 μg/ml) and G-418 (250 μg/ml). 2×10^4 cells/well were seeded in microplates and incubated overnight in 37 °C and 5% CO_2 before filibuvir was added. Filibuvir, VX-222, and tegobuvir, serially diluted 1:5 in the same medium, were transferred to the cell plates. The medium was removed after 48 h incubation with compound, and the cells were lysed. Luciferase activity was measured according to the supplier's instruction (cat. No. 484-103, BioThema, Handen, Sweden). Inhibition was calculated by comparing the luciferase activity in untreated wells with wells containing inhibitors at different concentrations.

2.4. In vitro polymerase activity assay

The polymerase activity was determined in a buffer of 20 mM Tris–HCl, 100 mM ammonium acetate, 20 mM NaCl, 2.5 mM $MnCl_2$, 10 mM DTT, 2 mM CHAPS, pH 7.5. The primer/template was a self-primed, hairpin RNA (RNA-H3) with the sequence 5′-UUU UUU UUU UAG UCA GUC GGC CCGGUU UUC CGG GCC-3′ and biotinylated at the 5′-prime end (custom synthesis at Eurogentec). The reaction was carried out with 30 nM NS5Bd21, 83 nM RNA-H3, 50 μM GTP, 2.5 μM ^{3}H-ATP (55.5 kBq of 2-,5′-,8-^{3}H-ATP, 1.66 TBq/mmol, Perkin Elmer (Waltham MA, USA), made to 10 μL of 2.5 μM ATP with cold ATP), and 2 μM each of CTP and UTP, and 80 U/mL RNaseOUT. Unlabelled nucleotides and RNaseOUT were all from Invitrogen (Stockholm, Sweden).

The NS5Bd21 was mixed with the RNA-H3, GTP, CTP, UTP, and RNaseOUT in 90 μL of buffer. One micro liter of inhibitor in DMSO or DMSO control was added and mixed. Longer incubation than 5 min was not found to be necessary before the reaction was started with 10 μL of ^{3}H-ATP and incubated at room temperature for 2 h. The reaction was stopped by the addition of 100 μL of 0.5 M EDTA. Reaction mixture (185 μL) was transferred to a streptavidin labelled FlashPlate (Perkin Elmer, Waltham MA, USA) and incubated overnight. Radioactivity was then counted in a Wallac Trilux Microbeta (Perkin Elmer, Waltham MA, USA) scintillation counter.

2.5. Thermal stability analysis by differential scanning fluorometry

Protein structure stabilization by ligand binding was assessed by differential scanning fluorometry (DSF) (Lo et al., 2004) according to published procedures (Niesen et al., 2007). In brief, NS5Bd21 (final concentration 2 μM) was mixed with SYPRO orange (Invitrogen, Stockholm, Sweden) in a 50 mM Tris–HCl buffer, pH 7.5. The concentration of dimethyl sulfoxide (DMSO, Sigma–Aldrich Sweden AB, Stockholm, Sweden) was adjusted to 2% in all samples. The inhibitor (filibuvir, VX-222, or tegobuvir) was added to a final concentration of 10 μM prior to a 10–15 min incubation. The final reaction volume was 40 μl. The fluorescence was excited at 480 nm and read at 520 nM in a mini Opticon unit (Bio-Rad Sweden, Stockholm, Sweden). The temperature was increased by 0.5 °C/min, from 25 to above 80 °C. All experiments were performed in duplicates in white 48 well plates (Bio-Rad).

2.6. RNA-NS5Bd21 interaction analysis

2.6.1. In vitro synthesis of biotinylated RNA

Two DNA oligonucleotides (5′ ATTCGTTAATACGACTCACTATAG GG 3′ and 5′ GGCGATTGATGGTTATATAAAGGGAGTATCGCCCT ATAGTGAGTCGTATTA 3′) were used as templates for synthesis of 31 bases of biotinylated RNA. The primers were annealed in 50 mM Tris–HCl pH 7.4 and 100 mM KCl by heating to 100 °C and cooling down to room temperature. The RNA was synthesized using Riboprobe T7 kit (Promega, Madison WI, USA) according to the manufacturer's instructions. RNA was biotinylated by adding biotin-C14-CTP (Invitrogen, Stockholm, Sweden) to the reaction with a 9:1 ratio of CTP and biotin-C14-CTP. The synthesized RNA was purified with a standard phenol/chloroform extraction procedure. Unincorporated nucleotides were removed using PD SpinTrap G-25 spin columns (GE Healthcare, Uppsala, Sweden). The concentration was measured using a nano-drop spectrophotometer (ND-1000, NanoDrop Technologies Inc., Wilmington DE, USA).

2.6.2. Immobilization of RNA

Analysis of NS5B–RNA interactions were performed using a Biacore X100 instrument (GE Healthcare, Uppsala, Sweden). Streptavidin (Sigma–Aldrich Sweden AB, Stockholm, Sweden) was diluted to 100 μg/ml in coupling buffer (10 mM NaAc pH 4.6, 0.1 mM EDTA, 1 mM NaCl, 1 mM DTT) and immobilized on CM5 chip surfaces by standard amine coupling; 8 min injection of an N-ethyl-*N*′-(3-dimethylaminopropyl)-carbodiimide (EDC) and *N*-hydroxysuccinimide (NHS) mixture, protein injection, and an 8 min ethanol amine injection (all reagents from GE Healthcare), to a final immobilization level of 4500 RU. The surface was washed 3 times with conditioning solution (1 M NaCl, 50 mM NaOH) to remove excess of unbound streptavidin. Biotinylated RNA was diluted to 500 nM in RNA immobilization buffer (10 mM Tris–HCl pH 8.0, 50 mM NaCl, 1 mM EDTA, 1 mM β-mercaptoethanol, and 0.005% (v/v) Tween20 (VWR Sweden, Stockholm, Sweden)) and captured on the streptavidin surface. All steps were performed at 25 °C.

2.6.3. Interaction experiments

Interaction experiments involving RNA and NS5B were performed essentially as described previously (Simister et al., 2009). NS5Bd21 was diluted in the running buffer (10 mM Tris–HCl pH 8.0, 150 mM NaCl, 1 mM DTT, 5% glycerol, and 0.05% (v/v) Tween20) in twofold serial dilution series ranging from 6.25 to 200 nM. The inhibitors were mixed with the protein in the concentration series to a final concentration of 300 nM for filibuvir and 900 nM for VX-222 prior to injection. The DMSO concentration in the protein running buffer was adjusted accordingly. The enzyme/inhibitor mixture was injected over the chip surface with immobilized biotinylated RNA. Blank samples of running buffer were injected for reference purposes. The surface was regenerated with a solution of 2 M NaCl and 2 M $MgCl_2$ after each cycle.

To validate the results, NS5Bd21 was immobilized by amine coupling on a CM5 chip (see below) over which a concentration series of RNA (twofold dilutions, 0.5–8 μg/ml) with a fixed 300 nM concentration of VX-222 or filibuvir was injected.

All buffers were prepared in diethylpyrocarbonate (DEPC) (Sigma–Aldrich Sweden AB, Stockholm, Sweden) treated water, filtered and degassed. Tween20 was the detergent of choice since it has been reported not to reduce the activity of truncated NS5B (Yamashita et al., 1998). The data were evaluated with the BIAevaluation software (v. 4.1).

2.7. Inhibitor-NS5Bd21 interaction analysis

A Biacore T100 SPR biosensor instrument (GE Healthcare, Uppsala, Sweden) was used for kinetic characterization of the NS5Bd21-inhibitor interaction.

2.7.1. Immobilization of NS5Bd21

NS5Bd21 (80 μg/ml, in 10 mM MES pH 6.0) was immobilized onto the biosensor chip surface by standard amine coupling and as described for streptavidin (above). An extra injection of EDC/

NHS, followed by a spontaneous deactivation of the reactive groups of the surface through a >1 h buffer stand-by flow, was used to cross-link the protein (Markgren et al., 2001). PBS-P (10 mM phosphate, 2.7 mM KCl, 0.137 M NaCl from PBS tablets (Sigma–Aldrich Sweden AB, Stockholm, Sweden), and 0.05% (v/v) Tween20 was used as running buffer during the immobilization procedure.

The immobilization level was translated into a theoretical maximal signal (R_{max}) according to Eq. (1) (MW for molecular weight).

$$R_{max}^{theor} = \frac{MW_{filibuvir}}{MW_{NS5BD21}} \cdot R_{immobilized} \quad (1)$$

2.7.2. Interaction mechanistic and kinetic analysis

To investigate the mechanism of binding between filibuvir and VX-222 and NS5Bd21, the two inhibitors were injected separately for 25, 50, 100, and 220 s at a single concentration (156 nM) over the two types of immobilized surfaces. An inhibitor stock in DMSO was typically diluted into concentration series between 5 and 156 nM in running buffer (20 mM Tris pH 7.4 at room temperature, 130 mM NaCl, 0.05% (v/v) Tween20) to a final DMSO concentration of 3% (v/v), using twofold dilutions. Two or three blank samples were included in each series. The samples were injected over the protein surface for 75 or 90 s at 30 μl/min.

A competition experiment was performed with saturating concentrations of filibuvir and VX-222 (500 μM). The inhibitors were injected over NS5Bd21 separately and mixed. The signal levels were compared between the samples.

Raw data was processed according to standard procedures, including reference and blank subtraction along with solvent correction, to eliminate any artifacts such as non-specific binding and discrepancies in buffer composition (Pornillos et al., 2002). Thereafter, each concentration series was subjected to global non-linear regression in the Biacore T100 Evaluation software (GE Healthcare). The 1:1 Langmuir binding model (Scheme 1) was used in the analysis to extract the kinetic parameters. However, more complex models were also evaluated, e.g. the two-step (induced fit) (Scheme 2) and heterogeneous ligand models (not shown). The dissociation equilibrium constant (K_D) was calculated from the association and dissociation rate constants.

$$E + I \underset{k_d}{\overset{k_a}{\rightleftarrows}} EI \qquad K_D = \frac{K_d}{K_a} \quad \text{(Scheme 1)}$$

$$E + I \underset{k_d}{\overset{k_a}{\rightleftarrows}} EI \underset{k_{-2}}{\overset{k_{-2}}{\rightleftarrows}} E*I \qquad K_D = \frac{K_d}{K_a} \cdot \frac{K_{-2}}{K_{-2} + K_Z} \quad \text{(Scheme 2)}$$

Data visualization was performed with Spotfire decision site software (TIBCO, Palo Alto, CA USA).

2.7.3. Chemodynamic analysis

The effects of pH (7.0, 7.1, 7.2, 7.5, and 8.0) and ionic strength (30, 130, 230, and 500 mM NaCl, all at pH 7.5) on interactions with NS5Bd21 were assessed at 25 °C for filibuvir and VX-222 as above. Tegobuvir was analyzed at pH 7.4 and 130 mM NaCl.

2.7.4. Temperature dependence analysis

For the temperature dependence analysis, each concentration series was analyzed at every 5° from 5 to 35 °C, using a fresh protein surface for each temperature series. The temperature range was chosen as broad as possible to improve statistical fidelity (Zhukov and Karlsson, 2007). Replicate runs were performed on separate surfaces. Both native and cross-linked NS5Bd21 was analyzed accordingly. An untreated surface was utilized for referencing purposes. To verify the stability of immobilized NS5Bd21, an additional concentration series was occasionally run at 5 °C after the main temperature series. The pH of the running buffer for the interaction experiments was adjusted to 7.4 at room temperature. The pH of a Tris buffer is 7.8 at 35 °C, and 7.0 at 5 °C.

Table 1
Anti HCV replicative activity (ED_{50}), inhibition (IC_{50}) and effect on thermal denaturation (ΔT_m) of NS5Bd21 by filibuvir, VX-222 and tegobuvir, and interaction kinetic rate constants (k_a, k_d, k_2, k_{-2}), equilibration dissociation constants (K_D) and residence times (τ) for filibuvir and VX-222.[a]

	Filibuvir	VX-222	Tegobuvir
EC_{50} (nM)	200	5	3
IC_{50} (nM) [b]	>100	7	>100 000
ΔT_m (°C)	4	5	0
Interaction model	1:1 Langmuir	Two-step (induced fit)	
K_D (nM)	54 ± 12	25 ± 0 [c]	
k_a (M^{-1} s^{-1})	$1.2 \times 10^6 \pm 0.2 \times 10^6$	$1.1 \times 10^6 \pm 0.1 \times 10^6$	
k_d (s^{-1})	0.065 ± 0.012	0.044 ± 0.003	
k_2 (s^{-1})	N/A	$3.3 \times 10^{-3} \pm 0.5 \times 10^{-3}$	
k_{-2} (s^{-1})	N/A	$5.4 \times 10^{-3} \pm 0.9 \times 10^{-3}$	
τ (s)	15[d]	222 [e]	

[a] The interaction kinetic parameters were determined at 25 °C, pH 7.5, and 130 mM NaCl. Values are arithmetic means of results from two experiments.
[b] The standard deviations for the averages of the log(IC_{50}) values in this assay were about 0.2 log units.
[c] For a two-step interaction, $K_D = k_d/k_a \cdot k_{-2}/(k_{-2} + k_2)$.
[d] Residence time for a one-step interaction, $\tau = 1/k_d$.
[e] Residence time for a two-step interaction, $\tau = (k_d + k_2 + k_{-2})/(k_d \cdot k_{-2})$.

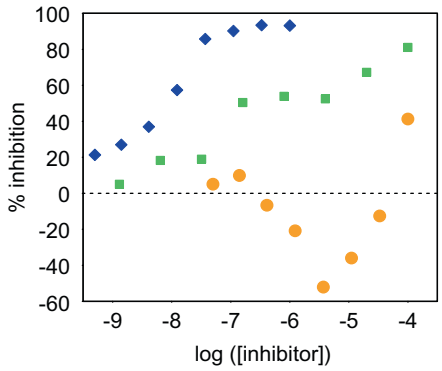

Fig. 2. Inhibition of the catalytic activity of NS5Bd21 as a function of inhibitor concentration for filibuvir (■), VX-222 (◆), and tegobuvir (●).

The dissection of the interaction between filibuvir and NS5Bd21 into the thermodynamic parameters entropy (ΔS) and enthalpy (ΔH) was achieved through the use of van't Hoff analysis. This has previously been described in more length, e.g. by Shuman et al. (2004).

In the simplest form, the affinity (K_D) can be expressed in terms of changes in entropy and enthalpy via changes in Gibbs free energy (ΔG) by combining Eqs. (2) and (3) into Eq. (4) (where '*R*' is the ideal gas constant and '*T*' is the absolute temperature).

$$\Delta G = \Delta H - T\Delta S \quad (2)$$

$$\Delta G = RTlnK_D \quad (3)$$

$$lnK_D = \frac{\Delta H}{RT} - \frac{\Delta S}{R} \quad (4)$$

This assumes, however, ΔS and ΔH to be temperature independent. The introduction of a temperature independent heat capacity (ΔC_P), as in Eq. (5a) and b, will, after integration, result in the expression in Eq. (6) (where α and β are integration constants).

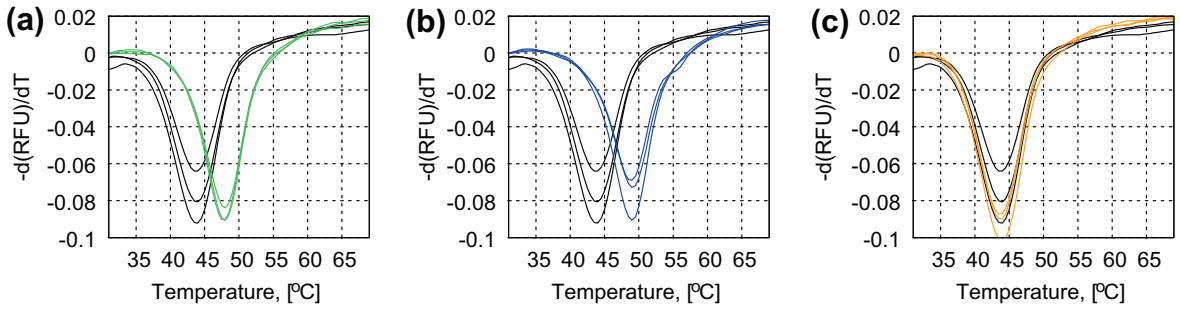

Fig. 3. Comparison of the thermal melting point (T_m) of NS5Bd21 in the absence (black) and presence (colour) of a ligand: (a) filibuvir, (b) VX-222, and (c) tegobuvir, measured using DSF and a SYPRO orange as reporter of unfolding. The rate of change in signal is plotted as a function of temperature and T_m values are read from the minima. Samples were run in triplicates.

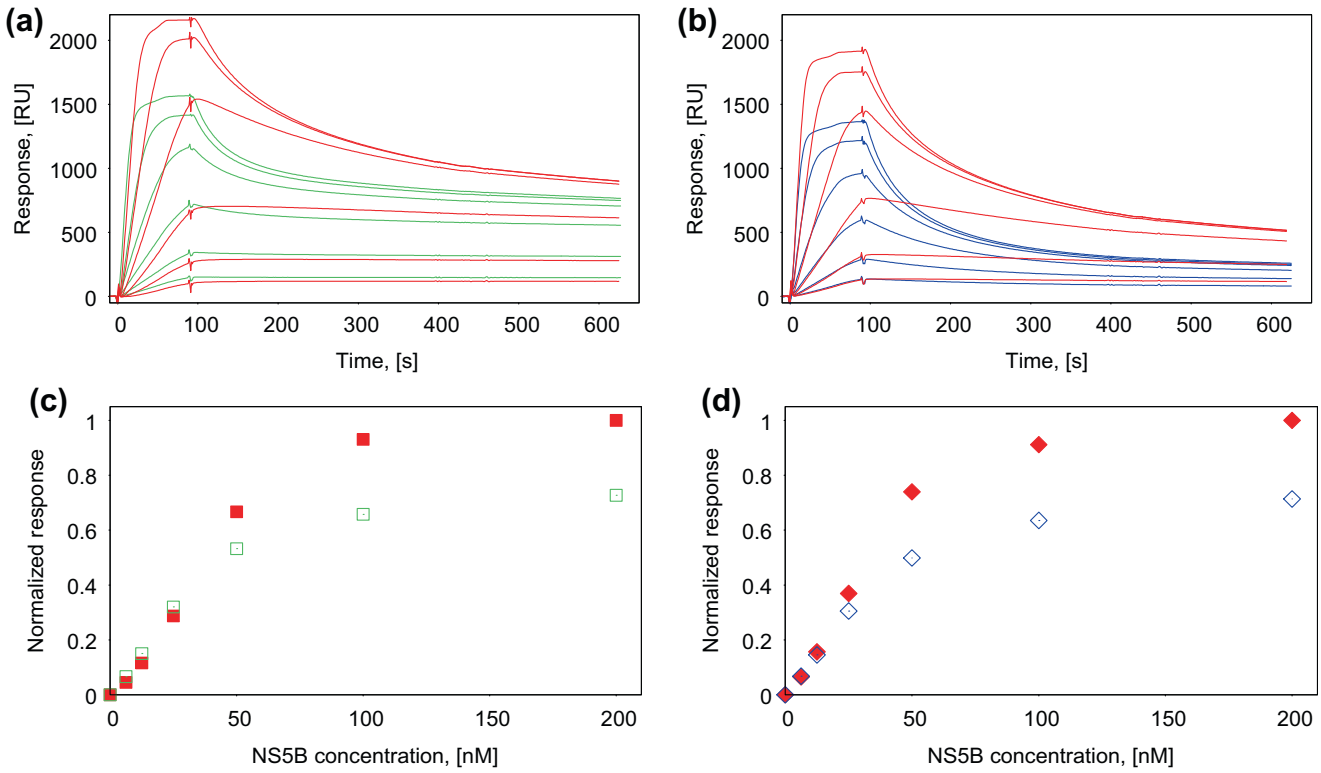

Fig. 4. Interaction between NS5Bd21 and immobilized RNA in the absence and presence of inhibitor. (a) 240 RU of RNA was captured via streptavidin and NS5Bd21 with 300 nM filibuvir first injected (green), followed by NS5Bd21 alone (red). (b) 200 RU of RNA was captured via streptavidin and NS5Bd21 with 900 nM VX-222 first injected (blue), followed by NS5Bd21 alone (red). The same concentration series of NS5Bd21 (6.25, 12.5, 25, 50, 100, and 200 nM) was used in both experiments. Sensorgrams were blank and reference subtracted. (c) and (d) show the concentration dependence of the signals at the end of the NS5Bd21 (filled markers) and NS5Bd21/inhibitor complex (open markers) injections as a function of enzyme concentration for filibuvir (squares) and VX-222 (diamonds), respectively. The response levels are normalized.

$$\frac{d(\Delta H)}{dT} = \Delta C_p \tag{5a}$$

$$\frac{d(\Delta s)}{dt} = \frac{\Delta C_p}{T} \tag{5b}$$

$$\ln K_D = \frac{1}{R}\left[\frac{1}{T}(\Delta C_p T + \alpha) - (\Delta C_p \ln T + \beta)\right] \tag{6}$$

The regression analysis using Eq. (6) together with affinity data from the biosensor experiments was performed in MATLAB (MathWorks, Natick MA, USA). The determined values of ΔC_P, α and β were used to calculate ΔH and ΔS of the complex formation.

Similarly, quasi-thermodynamic parameters for the association and dissociation events can be estimated by the method of Eyring through

$$\Delta G'_{on} = -RT\ln\left(K_a \frac{c \cdot h}{k_b \cdot T \cdot k}\right) \tag{7a}$$

$$\Delta G'_{off} = -RT\ln\left(k_d \frac{h}{k_b \cdot T \cdot k}\right) \tag{7b}$$

where 'C' is the state of the solvent (here set to 1 M), 'h' the constant of Planck, 'k_b' the Boltzmann constant, and 'κ' the transmission coefficient (here set to 1), to

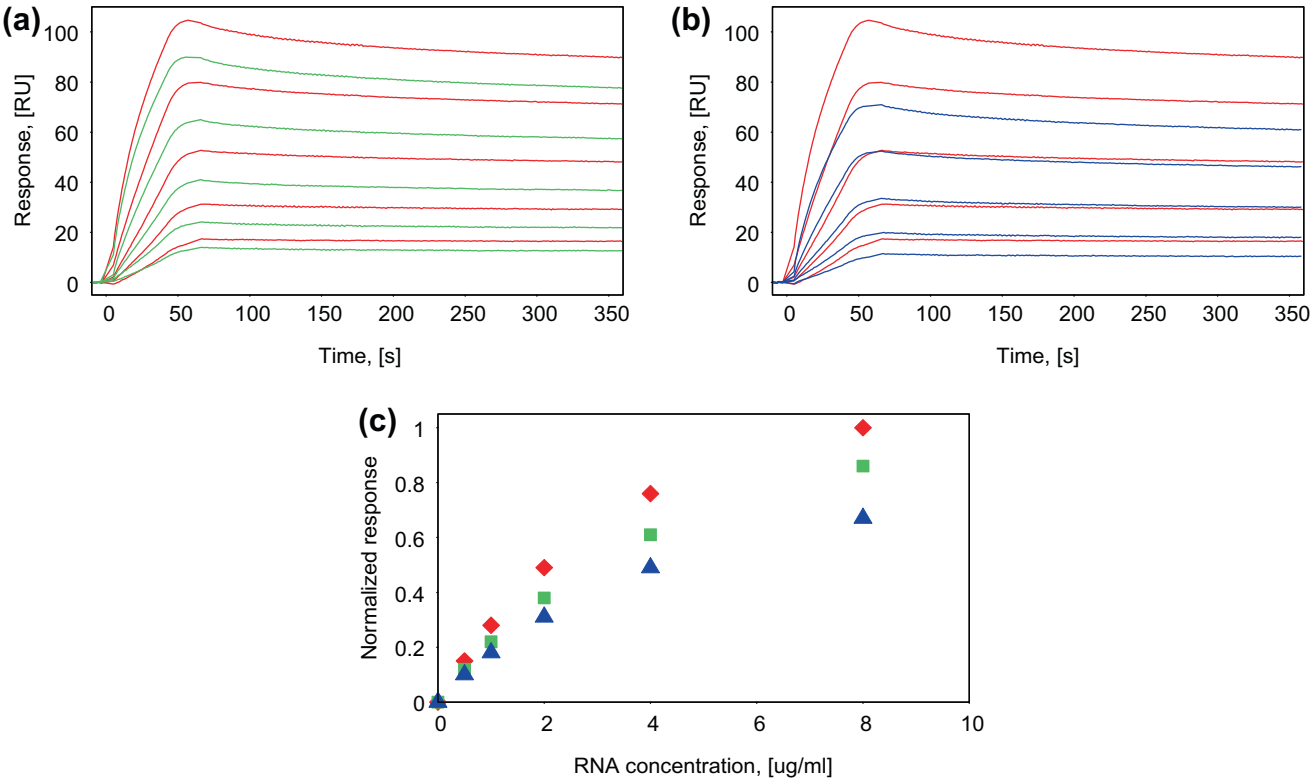

Fig. 5. Interaction between immobilized NS5Bd21 and RNA in the absence and presence of inhibitor. (a) RNA in the absence (red) and presence of 300 nM filibuvir (green). (b) RNA in the absence (red) and presence of 300 nM VX-222 (blue). RNA concentrations were 8, 4, 2, 1, and 0.5 μg/ml. (c) Signals at the end of RNA and RNA/inhibitor mixture injections as a function of polynucleotide concentration with RNA alone (♦), filibuvir (■) and VX-222 (▲). Sensorgrams are blank and reference subtracted in (a) and (b). Responses are normalized in (c).

$$ln\left(k_a \frac{c \cdot h}{k_b \cdot T \cdot k}\right) = -\frac{\Delta H'_{on}}{RT} + \frac{\Delta S'_{on}}{R} \quad (8a)$$

$$ln\left(k_d \frac{h}{k_b \cdot T \cdot k}\right) = -\frac{\Delta H'_{off}}{RT} + \frac{\Delta'_{off}}{R} \quad (8b)$$

The enthalpy and entropy can be calculated from their association and dissociation contributions as

$$\Delta H = \Delta H'_{on} - \Delta H'_{off} \quad (9a)$$

$$\Delta S = \Delta S'_{on} - \Delta S'_{off} \quad (9b)$$

3. Results

3.1. Anti HCV replicative effects

The inhibition of HCV replication in cell culture by filibuvir, VX-222, and tegobuvir were quantified as EC_{50} values (Table 1). The cytotoxicities of the inhibitors were lower than the EC_{50} values; all displayed $CC_{50} > 50$ μM, verifying that the EC_{50} values were attributable directly to effects on viral replication. However, the target or mode-of-action is not evident from this analysis. A series of additional experiments were required to resolve the differences in the effects of these compounds on HCV replication.

3.2. Inhibition of enzyme activity

Because the three compounds are known as NS5B polymerase inhibitors, their effect on the catalytic activity of NS5Bd21 was evaluated. VX-222 was identified as the most potent inhibitor, with an IC_{50} of 7 nM (Table 1). Filibuvir displayed a very shallow inhibition efficiency-to-inhibitor concentration curve with a Hill coefficient of 0.37 and only 80% inhibition at 100 μM inhibitor concentration (Fig. 2). This indicates that the inhibition is not simply due to a reversible one-step interaction mechanism and a meaningful IC_{50} value could therefore not be determined. Tegobuvir displayed an even more unusual curve, first stimulating the enzyme by up to 50% at 3.7 μM and then displaying 40% inhibition at 100 μM. This also indicates that the compound does not inhibit NS5B by a simple mechanism.

3.3. Effects on thermal stability of NS5B

As an initial evaluation of the mode-of-action of the three inhibitors, their effects on the thermal stability of NS5Bd21 were explored using differential scanning fluorimetry (DSF) and a fluorescent dye with affinity for hydrophobic parts of the protein (Lo et al., 2004). The experiment gives an indication of whether the compounds interact directly with the protein or not. Filibuvir and VX-222 resulted in a 4–5 °C increased melting temperature (T_m) of the enzyme. Tegobuvir was not observed to affect the T_m (Fig. 3).

3.4. Filibuvir and VX-222 interfere with the RNA binding of NS5Bd21

The influence of filibuvir and VX-222 on the interaction between NS5Bd21 and single stranded RNA was assessed by biosensor analysis in order to determine if their observed inhibition involved the interference of RNA binding to the enzyme. Biotinylated RNA was captured on biosensor surfaces to a level of 200–240 RU via immobilized streptavidin. NS5Bd21 was injected with and

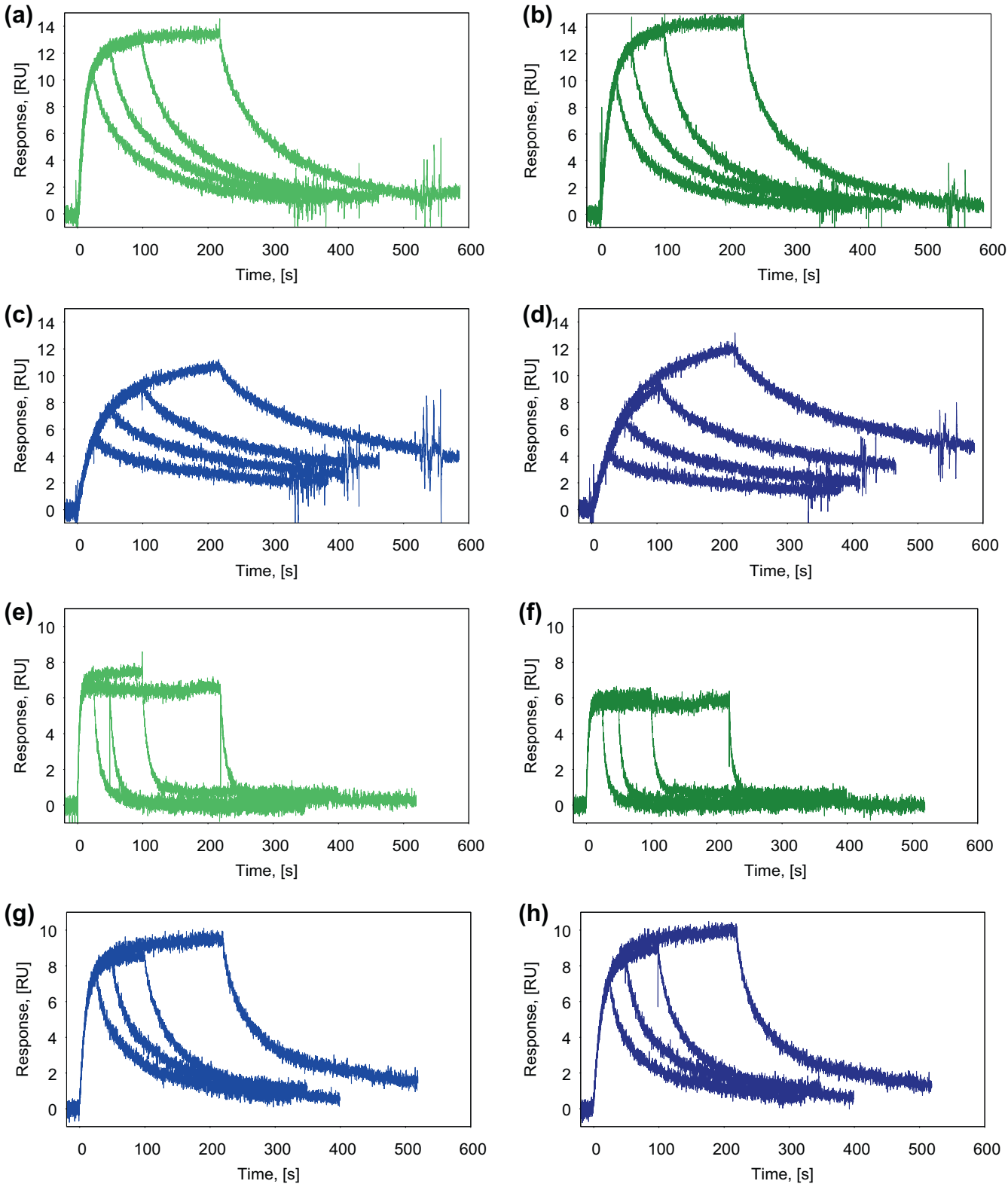

Fig. 6. Assessment of interaction mechanism of inhibitors by varying association phase length. Inhibitors were injected at 156 nM. Filibuvir (green; a–b, e–f) and VX-222 (blue; c–d, g–h) were injected at 5 °C (a–d) and 25 °C (e–h). Data were collected from native (light colours; a, c, e, g) and cross-linked (dark colours; b, d, f, h) enzyme surfaces. Sensorgrams are not normalized. (For interpretation of the references to colour in this figure legend, the reader is referred to the web version of this article.)

without saturating concentrations of each inhibitor and the interaction was monitored (Fig. 4a and b). The presence of either filibuvir or VX-222 clearly decreased the amount of RNA-enzyme complex formed, by approximately 30% at the highest concentration tested, as judged by the maximal signal level (Fig. 4c and d). However, the interaction was complex since the curves were not well described by any standard interaction model, and when injecting only NS5B, an interaction signal higher than the predicted R_{max} value was sometimes observed. The results were independent of injection order (not shown).

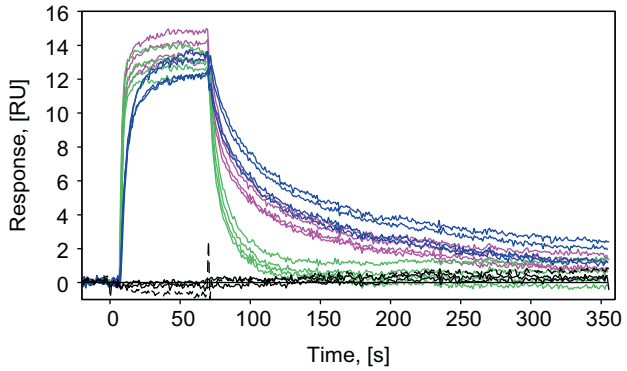

Fig. 7. Establishment of competition between filibuvir (green) and VX-222 (blue) for NS5Bd21 binding. The maximal response for a mix of inhibitors (magenta) equals those of the separate inhibitors. Blank samples are in black. The plot shows an overlay of 4 replicate sets, all run at 25 °C, pH 7.4. All individual inhibitor concentrations were 500 nM.

To validate the results, the experiment was turned around and NS5Bd21 was immobilized on a CM5 surface (approx. 2600 RU), where after a concentration series of non-biotinylated RNA was injected, first without and then with added inhibitor (300 nM of VX-222 or filibuvir) (Fig. 5). The maximal signal was again observed to be reduced by the presence of either of the inhibitors. Also this experiment shows that both filibuvir and VX-222 interfered with the ability of NS5B to interact with RNA, with VX-222 apparently having a slightly larger effect. In order to determine if the two inhibitors interact with NS5B with significantly different characteristics, an experimental design without RNA was required.

3.5. Determination of inhibitor interaction mechanisms and kinetic parameters

To further characterize the interaction between the inhibitors and their target, and to assess their interaction mechanisms, the inhibitors were injected for different lengths of time over native and cross-linked NS5Bd21 surfaces at a single concentration. No interaction between tegobuvir and the polymerase could be observed. It was therefore excluded from further experiments. The experiments with filibuvir and VX-222 were performed at 25 and 5 °C since the slower kinetics at the lower temperature facilitated a qualitative analysis. At 25 °C, the interaction between filibuvir and NS5Bd21 quickly reached an apparent steady state within the time frame of the experiment while the signal from VX-222 did not (Fig. 6e–h). At 5 °C, filibuvir did not reach steady state although it was closer to an apparent steady state than VX-222, showing a clear qualitative difference (Fig. 6a–d). Both inhibitors showed slight differences in the interactions with the native and cross-linked polymerase, most noticeable in the dissociation phases and for VX-222 also at the end of the association phases (Fig. 6c and d).

To determine if filibuvir and VX-222 compete for binding to NS5Bd21, a competition experiment was performed (Fig. 7). The responses for the inhibitors injected separately were not significantly different from the signal obtained when they were injected together as a mixture, confirming that they compete for binding to the enzyme. Note that this does not necessarily mean that they bind to the same site, simply that the binding of one compound influences the binding of the other. A qualitative difference in interaction kinetics between the inhibitors was observed.

The mechanism and kinetic parameters were determined for filibuvir and VX-222 at 25 °C by injecting a series of inhibitor concentrations over immobilized NS5Bd21 and globally fitting mechanistically reasonable interaction models to the data (Fig. 8). The kinetic parameters are presented in Table 1. For filibuvir, a simple reversible 1-step Langmuir interaction (Scheme 1) was adequate for description of the data (Fig. 8a). This mechanism was not suitable for VX-222 (Fig. 8b), for which a 2-step interaction mechanism (Fig. 8c) was superior. Also a heterogeneous interaction model (not shown) could be used for analysis of the interaction data for this inhibitor, but it was excluded for logical reasons (see discussion). A population shift model did not fit the data (not shown). The association and dissociation rate constants (k_a and k_d) for filibuvir and VX-222 were comparatively similar and the affinities (K_D) differed only by a factor of 2. Still, due to the second step of the VX-222 interaction, the residence time (τ) differed by more than a factor of 10.

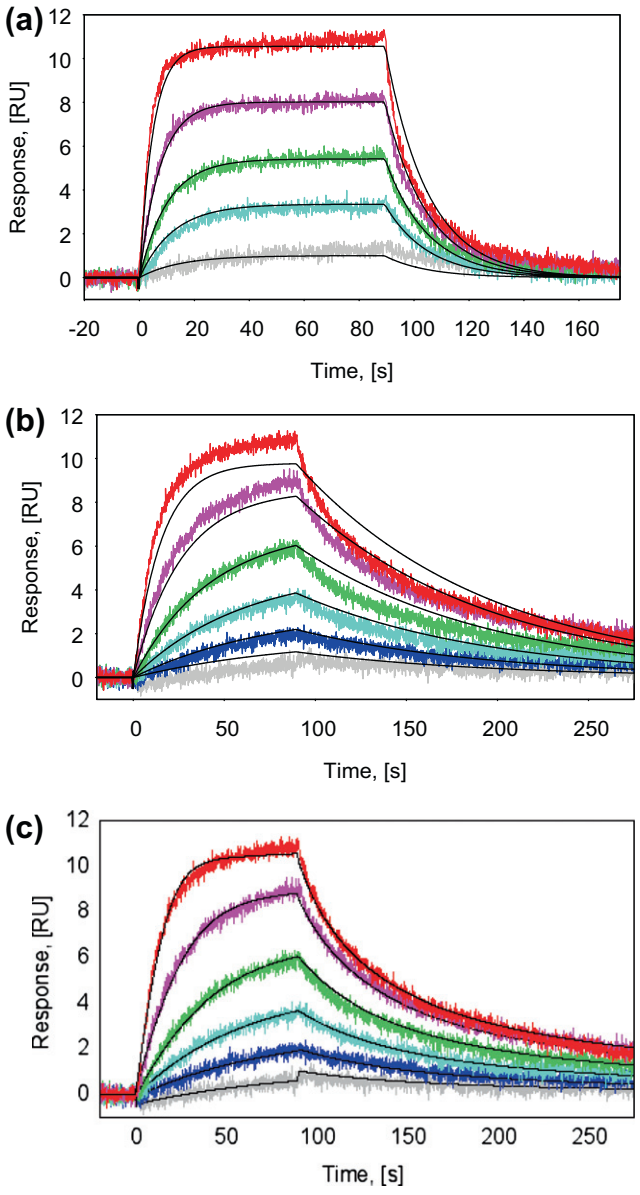

Fig. 8. Establishment of interaction mechanism and kinetic parameters for filibuvir (a), and VX-222 (b and c) interacting with NS5Bd21. Typical sensorgrams for experiments with compounds injected in two-fold concentration series between 5 and 156 nM (the 10 nM trace is excluded in a). Experimental traces are in colour and fitted models in black, with a Langmuir model used in a and b, and a two-step model in c. Experiments were performed at 25 °C. (For interpretation of the references to colour in this figure legend, the reader is referred to the web version of this article.)

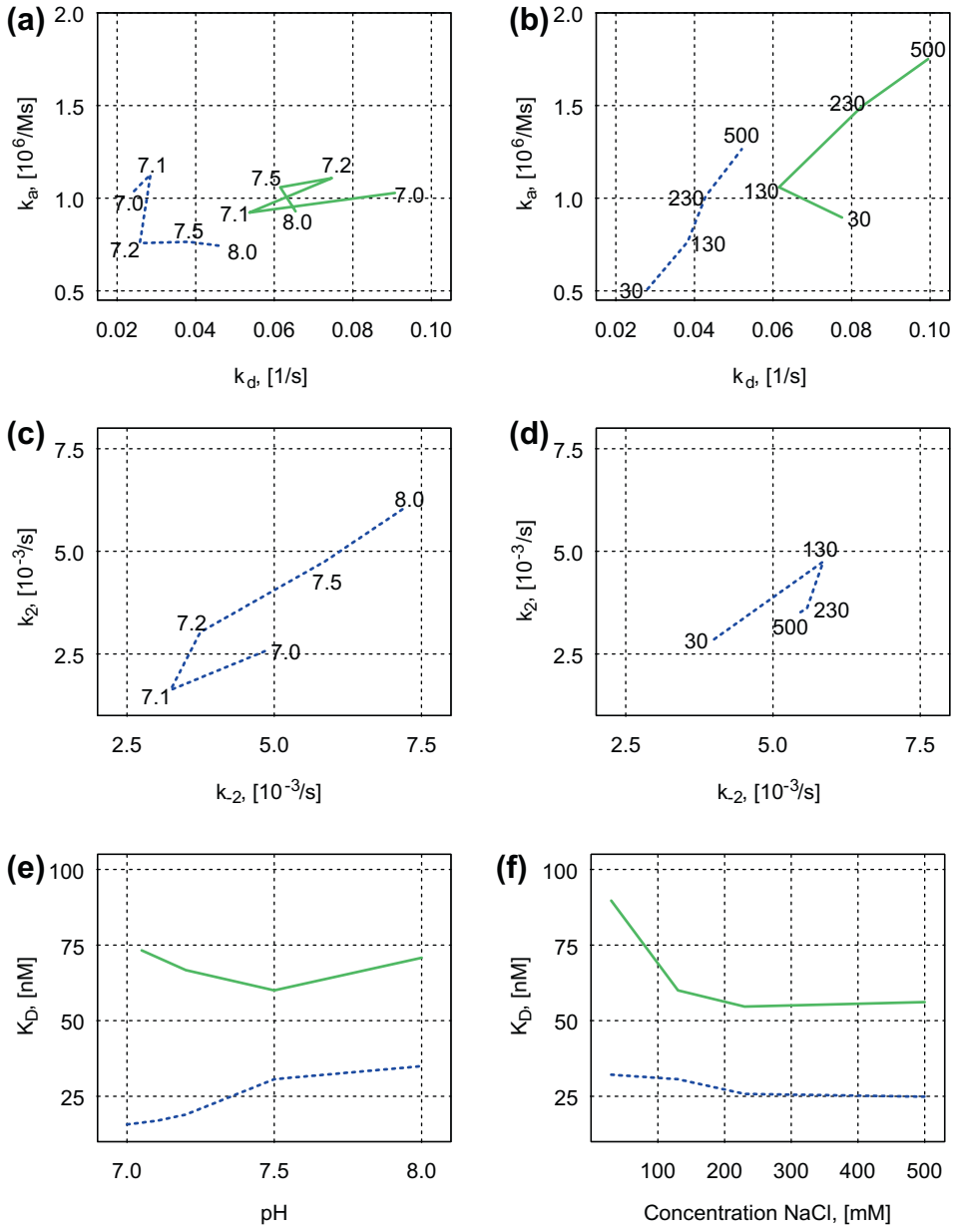

Fig. 9. Effect of buffer pH (left column of plots) and ionic strength (right column of plots) on association and dissociation rate constants (a) and (b) and equilibrium dissociation constant (e) and (f) of filibuvir (green) and VX-222 (blue, dashed line). The effect on the secondary rate constants for VX-222 of buffer pH and ionic strength are displayed in (c) and (d), respectively (cf. scheme 2). Values in figures are in pH units and mM NaCl. (For interpretation of the references to colour in this figure legend, the reader is referred to the web version of this article.)

3.6. Chemodynamic analysis: Interaction dependence on pH and ionic strength

To better understand the interaction characteristics of the two inhibitors, the effect of changing the buffer conditions was investigated. All filibuvir data were analyzed with the 1:1 interaction model and those of VX-222 with a two-step model. First, the pH dependence of the inhibitor interactions with NS5Bd21 was analyzed at five pH values between 7.0 and 8.0. No clear pH-effect trend was observed for filibuvir; neither for the kinetic rate constants, nor the equilibrium dissociation constant of the interaction (Fig. 9a and e, respectively). The interaction for VX-222 displayed a continuous, but modest, increase in K_D with increased pH (Fig. 9e). The k_2 and k_{-2} rate constants displayed an increasing linear trend above pH 7.1 (Fig. 9c).

The influence of ionic strength on the interaction was investigated by varying the NaCl concentration of the running buffer using four buffers containing between 30 and 500 mM NaCl, all at pH 7.5. A change from 30 to 130 mM NaCl increased the affinity of filibuvir through a small increase in k_a and a decrease in k_d. Above 130 mM, an overall equivalent increase in both k_a and k_d was observed, yielding an unaltered K_D value (Fig. 9f). VX-222 displayed an equivalent increase in k_a and k_d, and constant K_D value, across the NaCl gradient (Fig. 9b and f). Effects on k_2 and k_{-2} were very small (Fig. 9d).

3.7. Temperature dependence analysis: Thermodynamic profiling

To further characterize the interaction between filibuvir and NS5Bd21, concentration series of the inhibitor was analyzed at se-

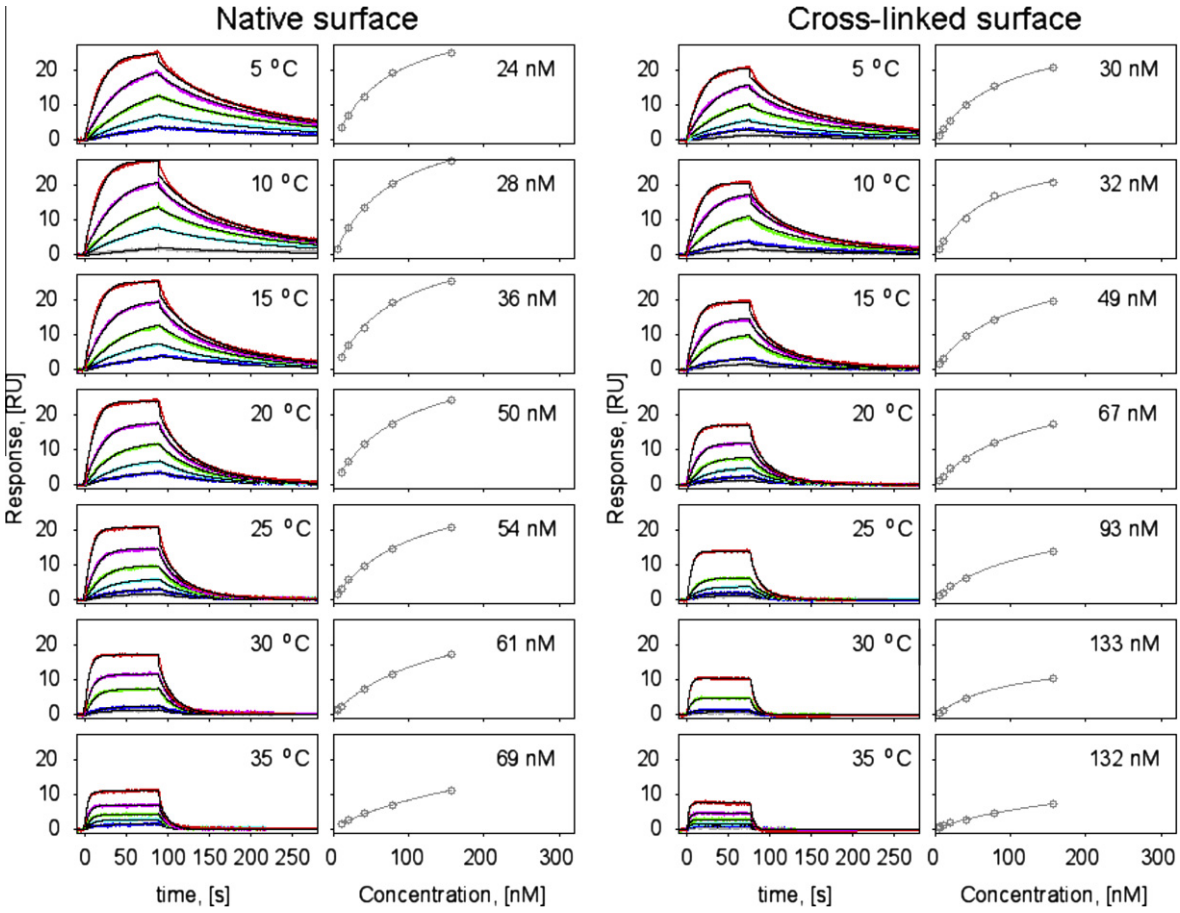

Fig. 10. Temperature-dependence analysis of NS5Bd21-filibuvir interactions. Coloured traces represent experimental data; the fitted Langmuir model is overlaid in black. Filibuvir samples were prepared in two-fold concentration series between 5 and 156 nM. Since some samples did not reach steady state and the highest concentration used was on the low end, the signal versus concentration plots should be considered to indicate trends. K_D values calculated by global non-linear regression from the sensorgrams are shown as insets. Sensorgrams have not been adjusted for different immobilization levels.

ven temperatures in the range of 5–35 °C with native and cross-linked, thus rigidified, NS5Bd21 (Fig. 10). The final immobilization level of the polymerase for these experiments was on average 4400 RU, corresponding to a theoretical R_{max} of 35 RU. The estimated R_{max} values from the regression analysis indicated an average of 50% apparent surface functionality at 25 °C. Both unaltered and cross-linked NS5Bd21 surfaces were used to investigate how the dynamic properties of the protein affected the interaction with the inhibitor. The decrease of pH with increasing temperature in the Tris buffers used was acknowledged but was deemed to have negligible effects on the kinetic rate constants (see above).

At low analysis temperatures, the sensorgrams for the native as well as the cross-linked surfaces were best described by a two-step model (Scheme 2) with a relatively slow k_{-2}. With higher temperatures, the 1:1 Langmuir binding model fitted increasingly better. This trend was more pronounced for the cross-linked surface. However, the 1:1 Langmuir interaction model was chosen for the estimation of kinetic parameters as a compromise since the values of the rate constants (k_a and k_d) and affinities for the formation of the encounter complex was similar to those determined with the more complex two-step model. The second step in the mechanistic scheme was therefore considered to be insignificant for this thermodynamic analysis. (The same assumption could not be made for VX-222, which was therefore not included in the thermodynamic analysis).

Replicate experiments confirmed that the assay was robust at all temperatures, giving high quality sensorgrams and similar parameter estimates. The observed R_{max} values from the regression analysis decreased with increasing temperature from 5 °C up to 35 °C, to increase again when the temperature was set to 5 °C anew, however not fully recovering to the initial level. Thus, the decrease was not a result of irreversible protein surface denaturation. The decline in R_{max} with temperature seems to be greater for unaltered NS5Bd21 compared to a cross-linked surface. However, with an apparent surface functionality of 50% during the cycles at 25 °C, the outcome of the interaction analysis should not be affected.

There was no clear correlation between the association rate constants and the analysis temperature, neither for the native nor the cross-linked surface (Fig. 11a). In contrast, the dissociation rate constants were linearly dependent on the temperature (Fig. 11b), with clear differences between the two types of protein surfaces; the k_d increased faster with increasing temperature for the cross-linked enzyme compared to the native. This translates into a corresponding temperature dependence also for the dissociation constant (K_D) (Fig. 11c), according to Eq. (1).

The K_D data were subsequently used for a linear (Fig. 11d) and a non-linear (plot not shown) van't Hoff analysis. The analysis resulted in fairly similar values of ΔS and ΔH (Fig. 12). The native NS5Bd21 surface displayed positive ΔS for binding of filibuvir compared to the slightly unfavorable change in entropy when binding to the cross-linked protein. Both enzyme types had favorable ΔH values, although more so for the cross-linked protein. Taken together, the overall changes in ΔG was quite similar for native and cross-linked NS5Bd21.

An Eyring analysis (see Eq. 8) of the association phase was not feasible due to the high variance of k_a (Fig. 11a), but the dissocia-

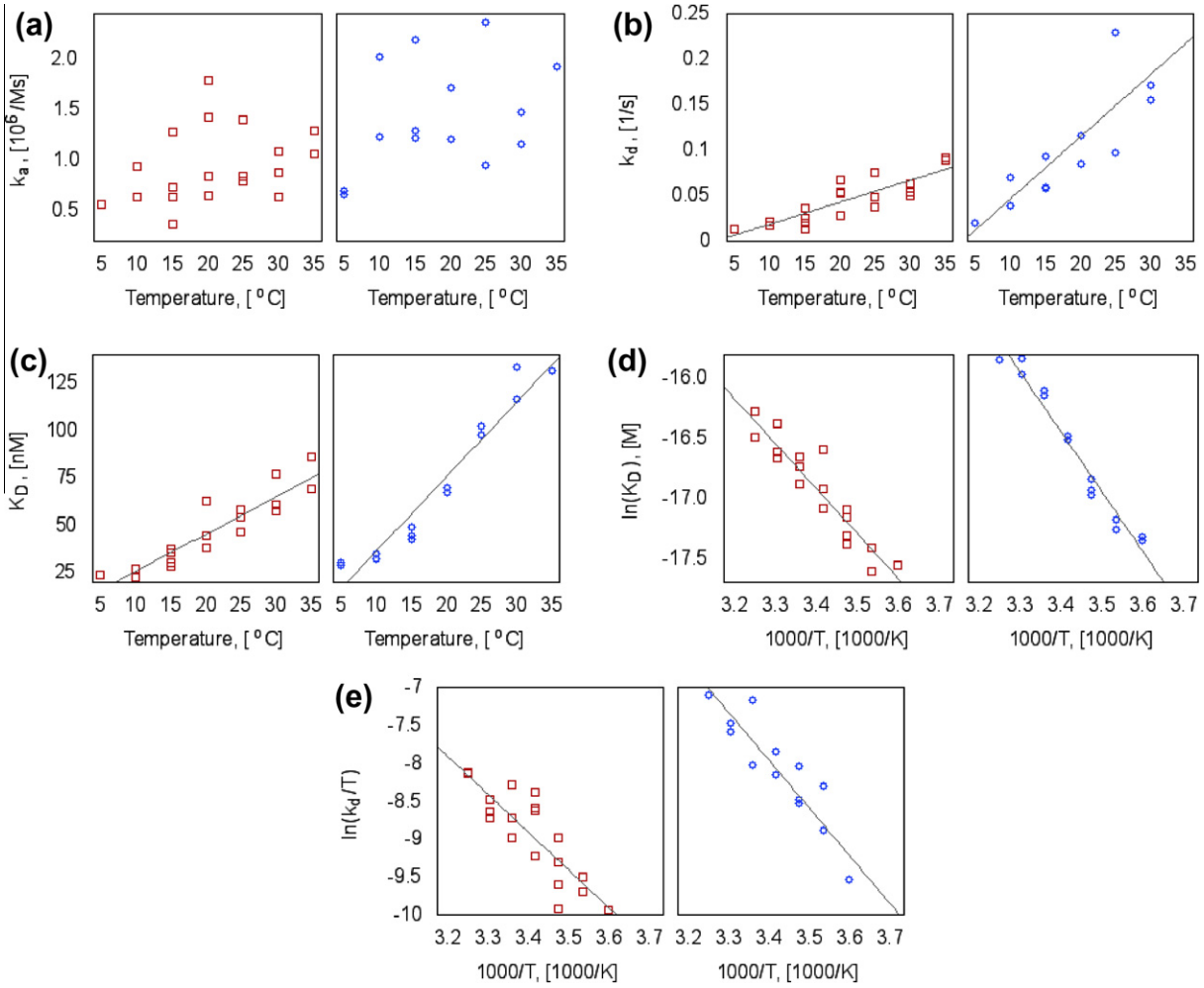

Fig. 11. Overview of kinetic parameters from the Langmuir binding model fit as a function of temperature. The relationship between temperature and association (a) and dissociation (b) rate constants, and the affinity (c) is shown. Plot (d) represent a linear van't Hoff analysis plot, and (e) an Eyring analysis of the dissociation rate. Experiments with native NS5Bd21 sensor surfaces in red squares to the left, with cross-linked in blue circles to the right. (For interpretation of the references to colour in this figure legend, the reader is referred to the web version of this article.)

tion phase could be examined (Fig. 11e). This revealed the enthalpic and entropic contributions shown in Fig. 12. The total interaction between filibuvir and NS5Bd21 display a negative enthalpy for both native and cross-linked enzyme. The former has a positive entropic contribution whereas the latter a small negative. For the dissociation event, both enzyme surface types displays positive (i.e. unfavorable) enthalpic and negative (i.e. unfavorable) entropic contributions, summarized in a large positive (unfavorable) change in free energy of the system. Through use of Eq. (9a) and b, the thermodynamic contributions for the association phase could be calculated, displaying a similar profile as for the dissociation phase.

4. Discussion

The interactions between the three clinical phase II candidates filibuvir, VX-222, and tegobuvir, and their drug target, the RNA dependent RNA polymerase of HCV, were explored in order to understand their inhibition mechanisms and differences in anti HCV replicative efficacy. The different anti-HCV replicative activity of filibuvir and VX-222 in cells, is in agreement with previously reported values for the genotype 1b Con1 strain (Yi et al., 2012, and references within), although filibuvir was found to be a little less potent than expected.

Even though tegobuvir was confirmed to be a potent inhibitor of HCV replication in replicons, it did not inhibit the enzyme in a biochemical assay and it was not found to interact with the enzyme in either DSF or SPR-based assays. Although the β-hairpin loop of NS5B genotype 1b (amino acids 435–455) has been identified to be important for the anti-HCV replicative activity of the inhibitor in a replicon system, it has been speculated that tegobuvir inhibits the polymerase via an indirect mode-of-action (Shih et al., 2011). During the course of this work, it has been shown that tegobuvir undergoes a CYP-mediated intracellular activation step, forming a glutathione conjugate that interacts covalently with NS5B (Hebner et al., 2012). This is consistent with our finding that un-activated tegobuvir is not able to interact with the target.

In contrast, DSF and SPR-based experiments confirmed that filibuvir and VX-222 both interacted directly with NS5Bd21. The two inhibitors are reported to be thumb-II site ligands (Legrand-Abravanel et al., 2010, and references within), which is in agreement with the observation that the inhibitors competed for binding to NS5Bd21. Moreover, both compounds were found to reduce RNA binding to NS5Bd21, with VX-222 being slightly more effective in one of the experimental setups. Although the inhibitors clearly interfere with the enzyme-RNA interaction, they do not block the interaction completely even at saturating concentrations. This is consistent with a recent molecular dynamics simulation that suggests that upon binding of the allosteric inhibitor to the thumb pocket, the polymerase can undergo a conformational change, which narrows the space between the finger and thumb

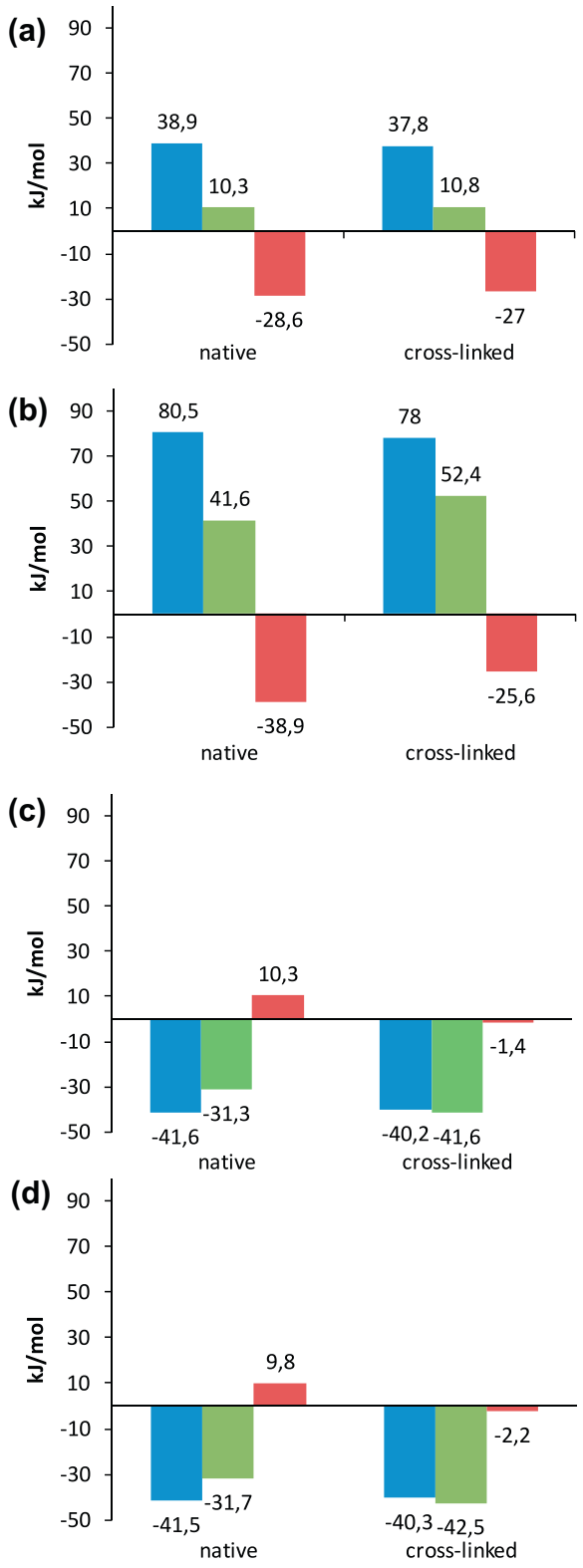

Fig. 12. Thermodynamic profiles of filibuvir-NS5Bd21 interaction for (a) the association, and (b) the dissociation events separately, and (c) at equilibrium according to a linear van't Hoff analysis, all at 25 °C. (d) The equilibrium profile as calculated by non-linear van't Hoff analysis at 25 °C. All units in kJ/mol. Bars from left to right: ΔG in blue, ΔH in green, and $T\Delta S$ in red. (For interpretation of the references to colour in this figure legend, the reader is referred to the web version of this article.)

domains. This may prevent the binding of the RNA to the active site of the enzyme (Davis and Thorpe, 2012).

The interactions between NS5Bd21 and RNA could not be mechanistically resolved due to higher order interactions. These can, for example, be a result of multiple enzyme molecules binding the same RNA strand, aggregation or oligomerization of NS5Bd21. Nevertheless, the data is in agreement with the observation that the two inhibitors first and foremost inhibit elongative RNA synthesis and that VX-222 has a modest effect on *de novo* initiation, whereas filibuvir has no obvious effect on that process (Yi et al., 2012). Since interference with RNA binding is expected to also inhibit *de novo* initiation, it is not clear if the differences between filibuvir and VX-222 in this study are in line with the previous report.

Due to the difference in anti HCV replicative effect of filibuvir and VX-222, we were interested in resolving the differences in the details of the interactions between the inhibitors and their target. The filibuvir interaction was readily described by a 1:1 Langmuir interaction model at all conditions tested, except at low temperatures. The observed lack of equilibrium at 5 °C, for example, suggests that there is a second step involving a conformational change that becomes rate limiting at low temperatures. This more complex interaction was observed for VX-222 under all conditions. Alternative models for VX-222 were excluded since the protein was judged to be pure by SDS–PAGE (not shown) and the results does not suggest that the inhibitor interacts with multiple binding modes. Both the effect of temperature on the complexity of the interaction and the effect of cross-linking support the interpretation that the interaction is influenced by the structural flexibility of the protein.

The chemodynamic analysis of filibuvir and VX-222 interactions with NS5Bd21 showed that they were both relatively insensitive to changes in buffer pH and ionic strength (i.e. concentration of NaCl) in the ranges tested (pH 7.0–8.0; 30–500 mM NaCl). The apparent differences are close to the experimental error and should therefore not be over interpreted. This indicates that the interaction forces involved in the binding of the compounds are similar, as expected if they bind to the same binding site and have similar hydrophobic/hydrophilic and electrostatic characteristics.

Filibuvir was further studied by temperature series in order to profile the interaction thermodynamically. The K_D and k_d values of filibuvir were found to increase linearly with increasing temperature. Thus, it was unexpected not to find a clear temperature dependence for k_a, considering the relationship between equilibrium and rate constants. However, a higher variability of the results is expected in the association event, compared to those of the dissociation phase, since it is affected by sample concentration. The cross-linked enzyme and the native enzyme differed in the magnitude of temperature dependence, suggesting that dynamics in the protein structure had an effect.

The K_D values were used for linear and non-linear van't Hoff analysis. The results agreed very well with each other. This suggests low temperature dependence of the thermodynamic entities, i.e. a small ΔC_p. The equilibrium for formation of the enzyme-inhibitor complex was found to be enthalpically favorable for both forms of the protein, and entropically favorable for the native polymerase but unfavorable for the cross-linked protein. The change in Gibbs free energy was, however, similar ($\Delta\Delta G = -1.4$ kJ/mol according to the linear van't Hoff analysis). Upon filibuvir binding, ΔS is expected to have a negative contribution from the joining of two molecules into one complex. However, the release of water molecules otherwise locked into the hydrophobic thumb-II pocket will have a positive contribution. The cross-linking may have affected this. By computing the vibrational entropy of α carbon atoms, it was concluded that the overall flexibility of the enzyme is reduced when an inhibitor is bound (Davis and Thorpe, 2012). The induced fit is therefore a likely mechanism of allosteric inhibitor binding to the thumb pocket.

Notably, the thermodynamic profile of the interaction between filibuvir and NS5B was similar to that reported for an allosteric inhibitor interacting with HIV reverse transcriptase, another viral polymerase (Geitmann and Danielson, 2007), but distinctly different to that for active site binding inhibitors of HIV protease (Shuman et al., 2004). Although it is still uncertain how time resolved thermodynamic profile of inhibitors interacting with their targets should be interpreted in structural/mechanistic terms, this new data set is an important contribution to the collection of ligand-target data sets that is expected to be valuable for future comparative purposes.

5. Conclusions

Tegobuvir was excluded as an NS5B ligand, leaving its mode-of-action unresolved. The difference in anti HCV replicative efficacy of filibuvir and VX-222 is not readily rationalized by using enzyme inhibition data or even affinities for the direct interaction, seeing that the affinities for NS5Bd21 were in the two-digit nanomolar range for both filibuvir and VX-222 and the formation and dissociation rates of the encounter complex for filibuvir and VX-222 with NS5Bd21 were similar. Clearly the differences must be rationalized on the basis of differences in their interaction mechanisms or kinetics. We hypothesize that the difference in binding mechanism between the two inhibitors is the cause. The most obvious difference is the induced fit mechanism proposed for VX-222 but not for filibuvir. It gives VX-222 a kinetic advantage since the residence time for VX-222 is 15 times longer compared to filibuvir despite their quite similar encounter complex formation rate constants and affinities. In addition, it appears that VX-222 was more efficient than filibuvir in interfering with the catalytic activity of the enzyme, as evidenced by the large difference in inhibitory effect despite similar affinities. This consequently gives VX-222 an additional mechanistic advantage over filibuvir.

Acknowledgements

The project has been funded by The Swedish Research Council (VR), the Sven and Lilly Lawski Scholarship fund (EA). Experimental work by Arne Müller is gratefully acknowledged.

References

World Health Organization HCV fact sheet, No. 164. 2011.
Beaulieu, P.L., 2010. Filibuvir, a non-nucleoside NS5B polymerase inhibitor for the potential oral treatment of chronic HCV infection. IDrugs: The Investigational Drugs Journal 13, 938–948.
Butt, A.A., Kanwal, F., 2012. Boceprevir and telaprevir in the management of hepatitis C virus-infected patients. Clinical Infectious Diseases: An Official Publication of The Infectious Diseases Society of America 54, 96–104.
Chayama, K., Hayes, C.N., 2011. Hepatitis C virus: how genetic variability affects pathobiology of disease. Journal of Gastroenterology and Hepatology 26 (Suppl. 1), 83–95.
Danielson, U.H., 2009. Integrating surface plasmon resonance biosensor-based interaction kinetic analyses into the lead discovery and optimization process. Future Medicinal Chemistry 1, 1399–1414.
Davis, B., Thorpe, I.F., 2012. Thumb inhibitor binding eliminates functionally important dynamics in the hepatitis C virus RNA polymerase. Proteins.
Elinder, M., Selhorst, P., Vanham, G., Öberg, B., Vrang, L., Danielson, U.H., 2010. Inhibition of HIV-1 by non-nucleoside reverse transcriptase inhibitors via an induced fit mechanism-importance of slow dissociation and relaxation rates for antiviral efficacy. Biochemical Pharmacology 80, 1133–1140.
Geitmann, M., Dahl, G., Danielson, U.H., 2011. Mechanistic and kinetic characterization of hepatitis C virus NS3 protein interactions with NS4A and protease inhibitors. Journal of Molecular Recognition 24, 60–70.
Geitmann, M., Danielson, U.H., 2007. Additional level of information about complex interaction between non-nucleoside inhibitor and HIV-1 reverse transcriptase using biosensor-based thermodynamic analysis. Bioorganic & Medicinal Chemistry 15, 7344–7354.
Geitmann, M., Unge, T., Danielson, U.H., 2006a. Biosensor-based kinetic characterization of the interaction between HIV-1 reverse transcriptase and non-nucleoside inhibitors. Journal of Medicinal Chemistry 49, 2367–2374.
Geitmann, M., Unge, T., Danielson, U.H., 2006b. Interaction kinetic characterization of HIV-1 reverse transcriptase non-nucleoside inhibitor resistance. Journal of Medicinal Chemistry 49, 2375–2387.
Granich, R., Crowley, S., Vitoria, M., Smyth, C., Kahn, J.G., Bennett, R., Lo, Y.R., Souteyrand, Y., Williams, B., 2010. Highly active antiretroviral treatment as prevention of HIV transmission: review of scientific evidence and update. Current Opinion in HIV and AIDS 5, 298–304.
Hebner, C.M., Han, B., Brendza, K.M., Nash, M., Sulfab, M., Tian, Y., Hung, M., Fung, W., Vivian, R.W., Trenkle, J., Taylor, J., Bjornson, K., Bondy, S., Liu, X., Link, J., Neyts, J., Sakowicz, R., Zhong, W., Tang, H., Schmitz, U., 2012. The HCV non-nucleoside inhibitor tegobuvir utilizes a novel mechanism of action to inhibit NS5B polymerase function. PLoS One 7, e39163.
Imhof, I., Simmonds, P., 2011. Genotype differences in susceptibility and resistance development of hepatitis C virus to protease inhibitors telaprevir (VX-950) and danoprevir (ITMN-191). Hepatology 53, 1090–1099.
Legrand-Abravanel, F., Nicot, F., Izopet, J., 2010. New NS5B polymerase inhibitors for hepatitis C. Expert Opinion on Investigational Drugs 19, 963–975.
Li, H., Tatlock, J., Linton, A., Gonzalez, J., Jewell, T., Patel, L., Ludlum, S., Drowns, M., Rahavendran, S.V., Skor, H., Hunter, R., Shi, S.T., Herlihy, K.J., Parge, H., Hickey, M., Yu, X., Chau, F., Nonomiya, J., Lewis, C., 2009. Discovery of (R)-6-cyclopentyl-6-(2-(2,6-diethylpyridin-4-yl)ethyl)-3-((5,7-dimethyl-[1,2,4]triazolo[1,5-a]pyrimidin-2-yl)methyl)-4-hydroxy-5,6-dihydropyran-2-on e (PF-00868554) as a potent and orally available hepatitis C virus polymerase inhibitor. Journal of Medicinal Chemistry 52, 1255–1258.
Lo, M.C., Aulabaugh, A., Jin, G., Cowling, R., Bard, J., Malamas, M., Ellestad, G., 2004. Evaluation of fluorescence-based thermal shift assays for hit identification in drug discovery. Analytical Biochemistry 332, 153–159.
Love, R.A., Parge, H.E., Yu, X., Hickey, M.J., Diehl, W., Gao, J., Wriggers, H., Ekker, A., Wang, L., Thomson, J.A., Dragovich, P.S., Fuhrman, S.A., 2003. Crystallographic identification of a noncompetitive inhibitor binding site on the hepatitis C virus NS5B RNA polymerase enzyme. Journal of Virology 77, 7575–7581.
Markgren, P.O., Lindgren, M.T., Gertow, K., Karlsson, R., Hämäläinen, M., Danielson, U.H., 2001. Determination of interaction kinetic constants for HIV-1 protease inhibitors using optical biosensor technology. Analytical Biochemistry 291, 207–218.
Niesen, F.H., Berglund, H., Vedadi, M., 2007. The use of differential scanning fluorimetry to detect ligand interactions that promote protein stability. Nature Protocols 2, 2212–2221.
Pornillos, O., Alam, S.L., Rich, R.L., Myszka, D.G., Davis, D.R., Sundquist, W.I., 2002. Structure and functional interactions of the Tsg101 UEV domain. The Embo Journal 21, 2397–2406.
Shih, I.H., Vliegen, I., Peng, B., Yang, H., Hebner, C., Paeshuyse, J., Purstinger, G., Fenaux, M., Tian, Y., Mabery, E., Qi, X., Bahador, G., Paulson, M., Lehman, L.S., Bondy, S., Tse, W., Reiser, H., Lee, W.A., Schmitz, U., Neyts, J., Zhong, W., 2011. Mechanistic characterization of GS-9190 (Tegobuvir), a novel nonnucleoside inhibitor of hepatitis C virus NS5B polymerase. Antimicrobial Agents and Chemotherapy 55, 4196–4203.
Shuman, C.F., Hämäläinen, M.D., Danielson, U.H., 2004. Kinetic and thermodynamic characterization of HIV-1 protease inhibitors. Journal of Molecular Recognition 17, 106–119.
Simister, P., Schmitt, M., Geitmann, M., Wicht, O., Danielson, U.H., Klein, R., Bressanelli, S., Lohmann, V., 2009. Structural and functional analysis of hepatitis C virus strain JFH1 polymerase. Journal of Virology 83, 11926–11939.
Vliegen, I., Paeshuyse, J., De Burghgraeve, T., Lehman, L.S., Paulson, M., Shih, I.H., Mabery, E., Boddeker, N., De Clercq, E., Reiser, H., Oare, D., Lee, W.A., Zhong, W., Bondy, S., Purstinger, G., Neyts, J., 2009. Substituted imidazopyridines as potent inhibitors of HCV replication. Journal of Hepatology 50, 999–1009.
Weislow, O.S., Kiser, R., Fine, D.L., Bader, J., Shoemaker, R.H., Boyd, M.R., 1989. New soluble-formazan assay for HIV-1 cytopathic effects: application to high-flux screening of synthetic and natural products for AIDS-antiviral activity. Journal of the National Cancer Institute 81, 577–586.
Yamashita, T., Kaneko, S., Shirota, Y., Qin, W., Nomura, T., Kobayashi, K., Murakami, S., 1998. RNA-dependent RNA polymerase activity of the soluble recombinant hepatitis C virus NS5B protein truncated at the C-terminal region. The Journal of Biological Chemistry 273, 15479–15486.
Yi, G., Deval, J., Fan, B., Cai, H., Soulard, C., Ranjith-Kumar, C.T., Smith, D.B., Blatt, L., Beigelman, L., Kao, C.C., 2012. Biochemical study of the comparative inhibition of hepatitis C virus RNA polymerase by VX-222 and filibuvir. Antimicrobial Agents and Chemotherapy 56, 830–837.
Zhukov, A., Karlsson, R., 2007. Statistical aspects of van't Hoff analysis: a simulation study. Journal of Molecular Recognition 20, 379–385.